CrystEngComm

PAPER

View Article Online
View Journal | View Issue

Cite this: *CrystEngComm*, 2015, **17**, 3089

Effect of substituents in the molecular and supramolecular architectures of 1-ferrocenyl-2-(aryl)thioethanones†

J. L. Ferreira da Silva,* Shrika G. Harjivan, André P. Ferreira, Karina Shimizu, M. Matilde Marques and M. Teresa Duarte

Received 22nd January 2015,
Accepted 8th March 2015

DOI: 10.1039/c5ce00149h

www.rsc.org/crystengcomm

We discuss here a comprehensive solid state approach to the influence of diverse molecular functionalities present in a group of 1-ferrocenyl-2-(aryl)thioethanones [aryl = phenyl, 2-, 3-, and 4-chlorophenyl, 3- and 4-methoxyphenyl, 4-nitrophenyl, and 2-naphthyl] on their molecular structures, intermolecular contacts and subsequent supramolecular arrangements. *Ab initio* calculations provide electrostatic charge distributions and electron density isosurface maps to assist this analysis. Atomic point charges are used to evaluate the best acceptors and donors in the molecules. The absence of good hydrogen donors increases the influence of close packing factors on the crystal network for the majority of these compounds. However the characteristics of each substituent, like the donor–acceptor ability of the methoxy group, electronic anisotropy of chlorine or electronic resonance of the nitro group, also play important roles in the self-assembly processes. A systematic and detailed analysis is presented.

Introduction

This paper reports analysis of molecular and supramolecular structures of a series of 1-ferrocenyl-2-(phenyl)thioethanones: unsubstituted 1-ferrocenyl-2-(phenyl)thioethanone (**I**) and 1-ferrocenyl-2-[(naphthalen-2-yl)thio]ethanone (**II**), methoxy substituted 1-ferrocenyl-2-[4-(methoxyphenyl)thio]ethanone (**III**) and 1-ferrocenyl-2-[3-(methoxyphenyl)thio]ethanone (**IV**),[1] chloro substituted 1-ferrocenyl-2-[4-(chlorophenyl)thio]-ethanone (**V**), 1-ferrocenyl-2-[3(chlorophenyl)thio]ethanone (**VI**) and 1-ferrocenyl-2-[2-(chlorophenyl)thio]ethanone (**VII**) and finally nitro substituted 1-ferrocenyl-2-[4-(nitrophenyl)-thio]ethanone (**VIII**) (Fig. 1).

In a previous paper,[1] we reported synthesis and characterization of a series of raloxifen-like 2-benzoyl-3-ferrocenylbenzo[*b*]thiophene derivatives containing several terminal alkylamino groups bonded to a benzoyl substituent, which displayed interesting activity against several tumor cell lines *in vitro*. Compound **IV**, an intermediate in the synthesis of these benzo[*b*]thiophene compounds, was prepared by a Friedel–Crafts-type acylation of ferrocene with chloroacetyl chloride, followed by a nucleophilic substitution with 3-methoxybenzenethiolate. The characterization of the novel organometallic benzo[*b*]thiophene derivatives and of intermediate **IV** included a preliminary study of the supramolecular arrangements of these compounds.

Analogous synthetic procedures, involving different benzenethiolates, were later used to prepare other 1-ferrocenyl-2-(aryl)thioethanones similar to **IV**, with the aim of preparing diverse starting materials for the synthesis of new raloxifene-like compounds and of studying the effect of different aryl substituents on their molecular and supramolecular structures. The focus of this paper is to understand how the introduced substituents interplay in the design and structural control of these particular molecular packing.

The eight molecules studied are all composed of a ferrocenyl group, an oxoethylthio bridge, and finally an aryl ring to which the different substituents are bonded. In terms of molecular interactions, the main feature of these

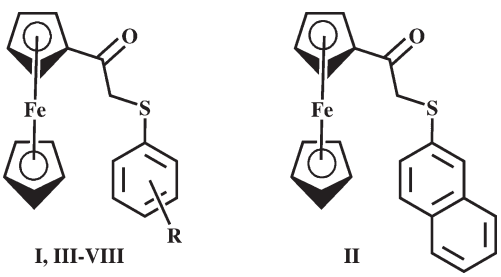

Fig. 1 Structures of the 1-ferrocenyl-2-(aryl)thioethanones discussed in the paper. **I**, R = H; **III**, R = 4-methoxy; **IV**, R = 3-methoxy; , R = 4-Cl; , R = 3-Cl; **VII**, R = 2-Cl; and **VIII**, R = NO_2.

Centro de Química Estrutural, Instituto Superior Técnico, Universidade de Lisboa, Av. Rovisco Pais, 1049-001 Lisboa, Portugal. E-mail: joao.luis@ist.utl.pt; Fax: +351 218417246; Tel: +351 218419282

† Electronic supplementary information (ESI) available. CCDC 1044508–1044513 and 1051170. For ESI and crystallographic data in CIF or other electronic format see DOI: 10.1039/c5ce00149h

molecules is the absence of hard hydrogen donors. The formation of hydrogen bonds is, therefore, almost limited to C–H···O interactions mainly with the carbonyl group, a group that is recognized as one of the best acceptors in this type of weak hydrogen bonds.[2] One of the objectives of this work is to establish that in this series of molecules, the C–H···$O_{carbonyl}$ interactions are determinant in the design of the supramolecular networks, an assumption commonly acknowledged in the absence of stronger donors and acceptors.[3,4]

The presence of a sulphur atom in the molecules creates the possibility of C–H···S and O=C···S interactions.[5–7] The aromatic rings present can be involved in C–H···π and π–π contacts.[8,9]

Introducing substituents with acceptor characteristics might create other regions in the molecules that are active for supramolecular interactions and can be strong competitors against the carbonyl group for the dominant role in the definition of the supramolecular arrangement. Our originally studied compound **IV** contained a methoxy group bonded to the *meta* position of the phenyl ring with its oxygen atom involved in C–H···O hydrogen bonds.[1] This study analyses the effect on the network that results from removing this substituent or moving it to the *para* position, as well as from inserting another good acceptor, the nitro group, in the same position. The other substituent to be examined is chlorine, a choice based on the various types of interactions in which this atom can get involved (C–H···X, type I and type II halogen bonds),[10–12] and their characteristic bonding parameters, whose high directionality[12] can strongly influence the crystal frameworks. Finally, we also discuss the effect of replacing the phenyl ring with the naphthyl group, which is a more extended aromatic system.

The electrostatic contribution to most of the mentioned intermolecular contacts suggests that the calculation of point charges for the atoms present in these molecules can be useful in the analyses of preferential interaction places. This estimate is achieved herein by DFT computations and the results are also used to represent electrostatic potential maps that can be utilized to explain repulsions between major molecular electronic density areas and their influence on the supramolecular structures.

Results and discussion

X-ray diffraction studies

Single crystal X-ray diffraction analysis allowed us to fully characterize the eight 1-ferrocenyl-2-(aryl)thioethanone compounds (Fig. 2 and 3). Some of their crystal parameters are reported in Table 1, while selected geometrical parameters are presented in Table 2 (see also Table S1 – ESI†). We have previously reported the molecular structure of compound **IV** and a preliminary survey of its supramolecular arrangement.[1] Nonetheless, the main features of **IV** are depicted in the tables and figures included in this section in order to achieve a complete comparison of the structural characteristics for the whole series of compounds analysed herein.

Bond lengths and angles are similar in all eight molecules and well within the expected range, as judged from extensive analysis of the values included in the CSD.[13,14] The main differences in the geometric parameters of the compounds lie in the relative values of the C(11)–C(12)–S(1)–C(13) torsion angle whose values range from 71 to 85° for compounds **I** to **VII**, while compound **VIII** exhibits values of 174–177° (see Table 2).

This angle defines the relative orientation between the aryl ring and the cyclopentadienyl (Cp) rings of the ferrocenyl moiety, a feature that divides these compounds in three classes: compound **I**, where the phenyl-containing moiety is rotated around the CH_2–S bond towards the unsubstituted Cp ring; compounds **II–VII**, in which the aromatic group also rotates around the same bond, but in the opposite direction, *i.e.* away from the unsubstituted Cp ring, and finally compound **VIII**, where a NO_2 group occupies the *para* position in the phenyl and the ring lies almost coplanar to the substituted Cp ring. The rationale for these different molecular orientations will be analysed together with the study of the supramolecular arrangements, since they are both based on the intra- and intermolecular contacts.

A notable structural feature that differentiates compounds **II** to **VII** is the angle β (see Fig. S1 – ESI†) between the plane of the aryl ring and the plane bisecting the ferrocenyl moiety (containing atoms C(1), Fe(1) and C(6)) that decreases from *ortho*- to *meta*-substituted compounds and from these to *para*-substituted compounds (see Table 2). Two arguments will be used to explain these differences: charge repulsion between the aryl and the carbonyl groups and steric hindrance; both will be addressed in the next section.

Electrostatic charge distribution

The electrostatic charge distributions in each compound were evaluated by *ab initio* calculations (see the Experimental section). These distributions were used to map electrostatic potentials onto electron density isosurfaces (Fig. 4) for the eight compounds. The calculated point charges for the individual atoms will be mentioned in the text whenever relevant and are displayed in totality in Table S2 (see the ESI†).

The skeleton of compounds **I** and **II** is limited to the ferrocenyl group, the bridge, and an aromatic group (phenyl or naphthyl). The aromatic groups contain the largest concentration of electronic density in these molecules, apart from the bridge (which includes the carbonyl group and a sulphur atom) (Fig. 4, **I** and **II**). In compound **II**, the larger aromatic ring results in both more pronounced steric restraints that prevent the folding of the molecule onto itself and higher charge density. In combination, these features force the naphthyl group to move away from the carbonyl, resulting in values of 144.51(37)° (molecule 1) and 147.06(31)° (molecule 2) for the β angle, as opposed to 129.30(9)° in compound **I**.

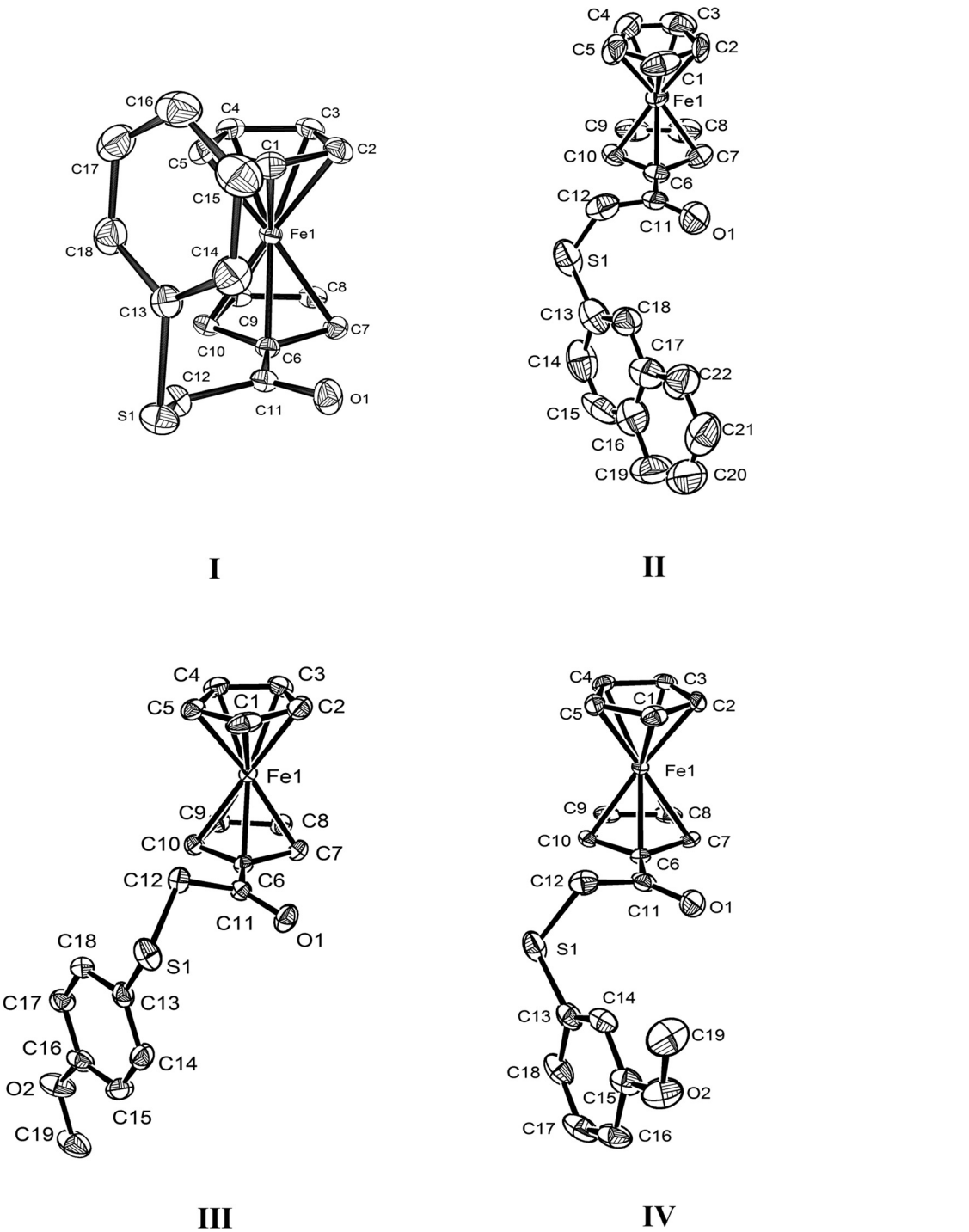

Fig. 2 ORTEP diagram, drawn with 50% probability ellipsoids, showing the atomic labelling scheme for 1-ferrocenyl-2-(phenyl)thioethanone (**I**), 1-ferrocenyl-2-[(naphthalen-2-yl)thio]ethanone (**II**), 1-ferrocenyl-2-[4-(methoxyphenyl)thio]ethanone (**III**) and 1-ferrocenyl-2-[3-(methoxyphenyl)-thio]ethanone (**IV**).[1]

Compounds **III** and **IV** have a methoxy group in the *para* and *meta* positions of the phenyl group, respectively (Fig. 2). Its oxygen atom displays a negative point charge (−41 and −40 atomic charge unit percentage (acu%) for **III** and **IV**, respectively) similar to that of the carbonyl oxygen (−50 acu% for both molecules) (Fig. 4), and therefore these two groups should repel each other. This effect is not very strong in **III**, due to the *para* position of the methoxy substituent, and so the β angle is smaller (133.17(7)°) than those observed in **I** and **II**; in **IV**, however, the *meta* substituent is closer to the carbonyl, compelling the phenyl ring to rotate and the angle between the two planes to open (155.68(8)°).

Compounds **V**, **VI** and **VII** have a chlorine atom occupying the *para*, *meta* and *ortho* positions in the phenyl ring,

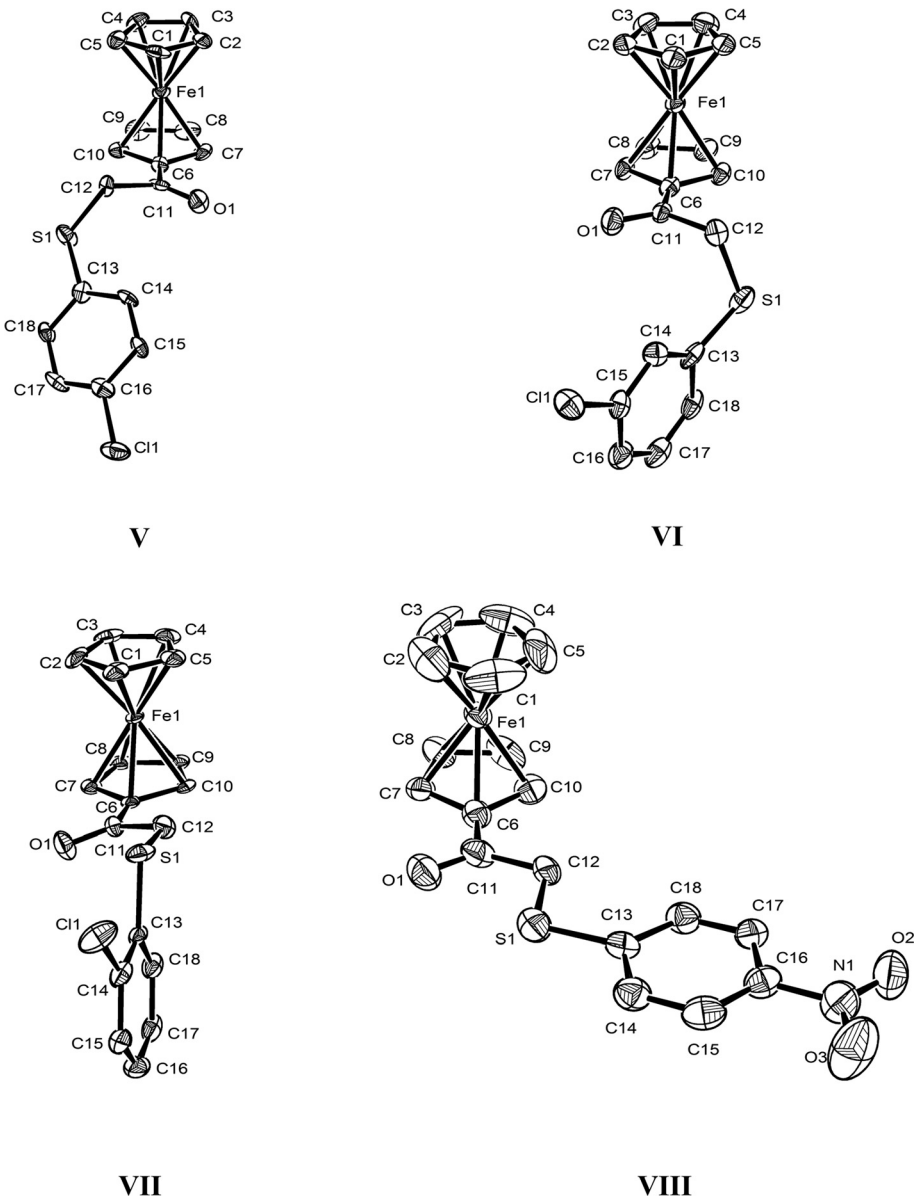

Fig. 3 ORTEP diagram, drawn with 50% probability ellipsoids, showing the atomic labelling scheme for 1-ferrocenyl-2-[4-(chlorophenyl)thio]-ethanone (**V**), 1-ferrocenyl-2-[3-(chlorophenyl)thio]ethanone (**VI**), 1-ferrocenyl-2-[2-(chlorophenyl)thio]ethanone (**VII**) and 1-ferrocenyl-2-[4-(nitrophenyl)thio]ethanone (**VIII**).

respectively. Two important conclusions can be drawn from Fig. 4, and the most noticeable one is that the chlorine atoms show a negative charge, although their point charges (−15, −14 and −11 acu%, respectively) are not as intense as those of the methoxy oxygens. The second feature is the anisotropic charge density at the halogen atoms, originally referred by Metrangolo *et al.*,[12] that consists of an electron deficient "cylinder" along the C–halogen bond axis (the area on the top of the atom in green), surrounded by an electronegative ring (the area in yellow). As for the methoxy substituted compounds, the β angle increases from the *para*- (115.06(27)–117.24(30)°) to the *meta*-substituted compound (142.09(20)°), with the larger value observed for the *ortho* compound (177.37(16)°). This trend can again be rationalized as a consequence of the growing repulsion between the carbonyl group and the chlorine. It should be noted that the angles for the *para*- and *meta*-substituted compounds are smaller with chlorine than those with methoxy substituents due, in part, to the higher point charges of the methoxy oxygens; in addition, the larger relative volume of the methoxy substituent may also be a factor.

The electron density surface of compound **VIII** (Fig. 4) shows the existence of two areas with a large density of electronic charge: the carbonyl oxygen and the nitro group. The main feature that distinguishes this molecule from the other seven is the almost planar arrangement of the entire atomic framework spanning from the substituted Cp to the nitro group. This group acts as a strong electron attractor by

Table 1 Crystal parameters for compounds I–VIII

	Chem. formula	Cryst. system	Space group	a (Å) b (Å) c (Å)	α (°) β (°) γ (°)	Z	Z'	Packing index (%)
I	$C_{18}H_{16}Fe_1O_1S_1$	Monoclinic	$C2/c$	18.895(5) 5.769(3) 26.820(6)	90 90.989(5) 90	8	1	71.9
II	$C_{22}H_{18}Fe_1O_1S_1$	Orthorhombic	$Pca2_1$	10.570(5) 7.329(4) 45.553(8)	90 90 90	8	2	68.6
III	$C_{19}H_{18}Fe_1O_2S_1$	Triclinic	$P\bar{1}$	5.706(3) 11.339(5) 13.634(5)	112.724(5) 94.083(8) 94.391(10)	2	1	71.1
IV[1]	$C_{19}H_{18}Fe_1O_2S_1$	Monoclinic	$P2_1/c$	21.5959(8) 7.3570(3) 10.2431(3)	90 97.571(2) 90	4	1	70.7
V	$C_{18}H_{15}Fe_1O_1S_1Cl_1$	Orthorhombic	$Pna2_1$	24.794(5) 5.846(3) 21.572(4)	90 90 90	8	2	70.7
VI	$C_{18}H_{15}Fe_1O_1S_1Cl_1$	Monoclinic	$P2_1/c$	7.6287(18) 23.333(6) 9.210(2)	90 108.146(9) 90	4	1	71.0
VII	$C_{18}H_{15}Fe_1O_1S_1Cl_1$	Monoclinic	$P2_1/n$	7.119(3) 23.6200(8) 9.661(2)	90 108.071(7) 90	4	1	71.3
VIII	$C_{18}H_{15}Fe_1O_3S_1N_1$	Monoclinic	$P2_1$	6.0532(19) 34.587(8) 7.827(2)	90 101.767(9) 90	4	2	[a]

[a] Could not be calculated due to disorder in the Cp ring.

Table 2 Selected geometrical parameters for compounds I–VIII

Angles (°)	I	II	III	IV	V	VI	VII	VIII
C(7)–C(6)–C(11)–C(12)	−179.38(18)	−4.1(14), −167.2(8)	157.44(13)	165.09(18)	167.3(7), −165.6(6)	178.5(5)	−164.7(4)	−171.4(8), 173.2(7)
C(10)–C(6)–C(11)–C(12)	7.0(3)	168.8(8), 7.5(14)	−17.8(2)	−9.0(3)	−4.6(9), 5.3(9)	−4.1(8)	9.4(6)	−1.3(13), 1.9(13)
C(11)–C(12)–S(1)–C(13)	74.00(17)	76.7(8), −76.8(7)	−71.04(12)	73.92(17)	85.3(5), −82.9(6)	−74.0(4)	78.9(3)	177.8(6), −174.8(6)
C(15)–C(16)–N(1)–O(3)	—	—	—	—	—	—	—	0.4(13), 3.0(10)
C(17)–C(16)–N(1)–O(2)	—	—	—	—	—	—	—	−0.8(13), 10.9(11)
C(15)–C(16)–O(2)–C(19)	—	—	−1.2(2)	—	—	—	—	
C(17)–C(16)–O(2)–C(19)	—	—	179.36(15)	—	—	—	—	—
C(16)–C(15)–O(2)–C(19)	—	—	—	−170.8(2)	—	—	—	—
C(14)–C(15)–O(2)–C(19)	—	—	—	8.9(3)	—	—	—	—
β [C(1)–Fe(1)–C(6)/-aromatic ring]	129.30(9)	144.51(37), 147.06(31)	133.17(7)	155.68(8)	115.06(27), 117.24(30)	142.09(20)	177.37(16)	79.88(35)[a]

[a] Could not be calculated due to disorder in the Cp ring.

both induction and resonance, thereby promoting the establishment of an extended conjugated π-system that causes the whole molecular moiety containing the phenyl ring to adopt this geometry.

Supramolecular arrangements

The structural characteristics of compounds **I–VIII**, the types of substituents present, and the point charges (see Table S2 – ESI†) indicate that the carbonyl oxygen is the strongest candidate for the best hydrogen bond acceptor, while only carbon atoms can act as hydrogen donors. So it is not surprising that weak C–H···$O_{carbonyl}$ hydrogen bonds are the main intermolecular interactions. The intermolecular contact structural parameters are listed in Table S3 (the ESI†).

1-Ferrocenyl-2-(phenyl)thioethanone (I). The electrostatic potential map of this compound (Fig. 4) displays an area with large electron density, involving the carbonyl group and the sulphur–methylene bridge and centred at the oxygen atom (−51 acu%).

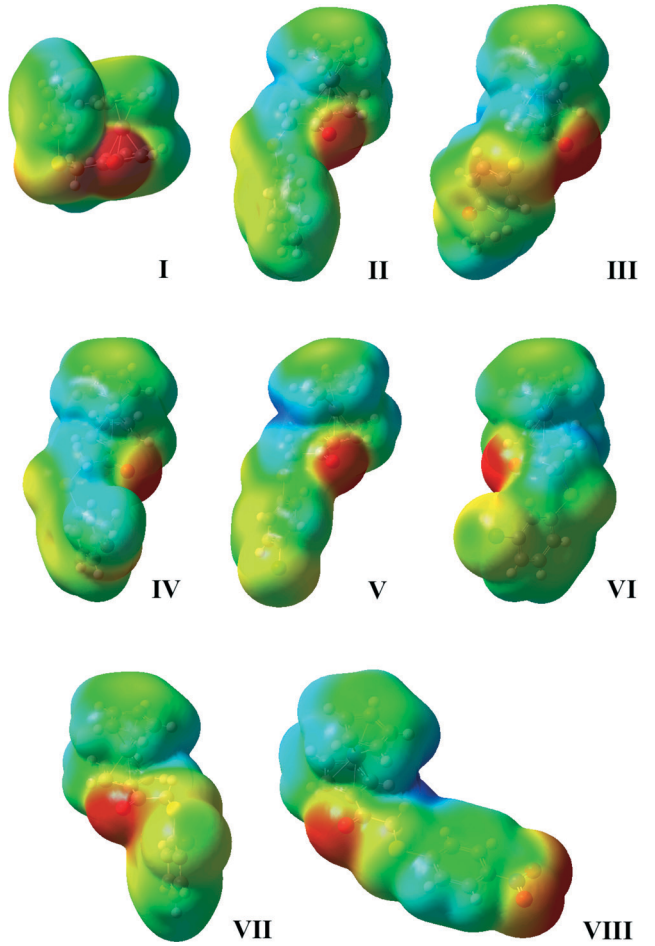

Fig. 4 Electrostatic potential mapped onto an electron density isosurface for compounds I to VIII. Positively or negatively charged regions are indicated by color gradients changing from blue to red, respectively.

The presence of a dispersed negative charge on the phenyl ring, together with the possibility of rotation of the S–phenyl group around the S(1)–C(12) bond, in order to leave the ring facing one C–H bond of the unsubstituted Cp ring, C(1)–H(1), enables the formation of a C_{Cp}–H$\cdots\pi_{Ph}$ intramolecular bond.

The formation of this intramolecular bond essentially explains the different molecular structures of this compound when compared to the others (**II–VIII**) included in this survey.

Compound **I** displays a supramolecular arrangement based on C_{Ph}–H$\cdots O_{carbonyl}$ C(7) chains, involving C(18)–H(18)$\cdots$O(1) hydrogen bonds (Fig. 5). DFT calculations show that H(5) is the hydrogen atom with a more positive point charge (+15 acu%), while H(18) displays a slightly smaller value (+11 acu%). Thus, the choice of donor atoms must be based on other factors besides electrostatic reasons. Had the C–H$\cdots O_{carbonyl}$ hydrogen bond involved the H(5) atom, the resulting structure would not be as compact (with a packing index (PI) of 71.9%).

The electrophilic character of the carbonyl C atom, C(11) (+50 acu%), brings about its participation in weak S$\cdots$C(π)=O interactions[7] (S(1) = −31 acu%) between two chains "growing" in opposite directions along *b* (as growing direction, we consider the orientation of the C_{Ph}–H$\cdots O_{carbonyl}$ hydrogen bonds). These double chains interact along *c* through parallel displaced π–π stacking interactions[9] involving the substituted Cp rings (Fig. 6).

1-Ferrocenyl-2-[(naphthalen-2-yl)thio]ethanone (II). Compound **II** is expected to present a similar supramolecular arrangement to that of **I**, because a non-substituted aromatic system is connected to the sulphur atom. As anticipated, the primary motif is again composed of linear C(7) chains formed by C_{aryl}–H$\cdots O_{carbonyl}$ hydrogen bonds, growing along *b*; however, as the compound displays $Z' = 2$, these chains are formed separately by type 1 and type 2 molecules (Fig. 7). Hydrogen atoms have very similar point charges, so the choice of those involved in the interactions is once again determined by their relative position, leading towards a more compact structure.[15]

The aromatic system in **II** is larger than that in **I**, favouring π interactions but imposing more steric restraints. Actually, a "V"-structured double chain is formed based on C_{aryl}–H$\cdots\pi_{aryl}$ interactions with type 1 molecules acting as hydrogen donors (Fig. 7 and S2†). In order to attain this herringbone arrangement, the S-aryl group rotates around the S(1)–C(12) bond, but in the direction opposite that observed in **I**, positioning the π-system away from the ferrocenyl group and allowing greater freedom for supramolecular interactions.

These "V"-chains align on top of each other in alternated directions, forming an angle of 81.8° between the axes of ferrocenyl moieties (see the ESI,† Fig. S3). The aromatic groups are not stacked, so this arrangement results mainly from $C_{methylene}$–H$\cdots\pi_{aryl}$ contacts.

1-Ferrocenyl-2-[4-(methoxyphenyl)thio]ethanone (III). Despite the presence of the methoxy group, the carbonyl oxygen remains the strongest hydrogen bond acceptor in this molecule. The supramolecular arrangement of the *para*-methoxy compound (**III**) involves, as a primary motif, the formation of a bifurcated[16] hydrogen bond: C_{Ph}–H$\cdots O_{carbonyl}$ and C_{Cp}–H$\cdots O_{carbonyl}$. This results from competition for the best acceptor between the two hydrogen atoms with higher point charges that are geometrically better positioned to engage in C–H$\cdots O_{carbonyl}$ hydrogen bonds, H(10) (18 acu%) and H(18) (13 acu%); these bifurcated hydrogen bonds form chains along *a* (Fig. 8 and S4†).

Two of these chains, growing in opposite directions, interact forming again a double chain, also along *a*, by means of $C_{methylene}$–H$\cdots O_{carbonyl}$ hydrogen bonds, reinforced by C_{Cp}–H$\cdots$S contacts (Fig. 8). So the oxygen atom of the carbonyl group is actually involved in a trifurcated hydrogen bond,[19] a situation explained by the H(12) point charge (12.8 acu%), the largest value found for methylene hydrogens in all the eight compounds studied.

The presence of a group that can act as both an acceptor and a donor will certainly influence the crystal packing of this compound. The growth on the *bc* plane is based on interactions that precisely involve the methoxy group: C_{Cp}–H$\cdots O_{methoxy}$ hydrogen bonds and $C_{methoxy}$–H$\cdots\pi_{Cp}$ short

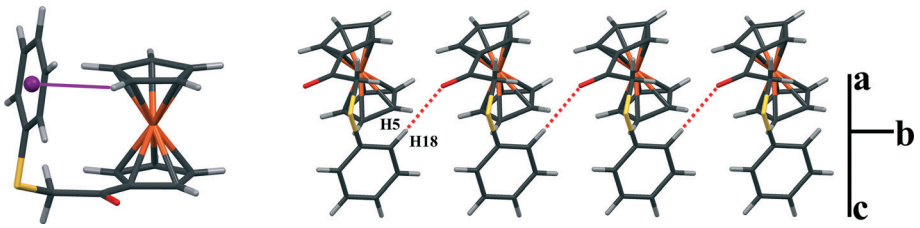

Fig. 5 Intramolecular C_{Cp}–H···π hydrogen interaction in **I** (left); chains of molecule **I** growing along *b* (right) through C_{Ph}–H···$O_{carbonyl}$ (in red).

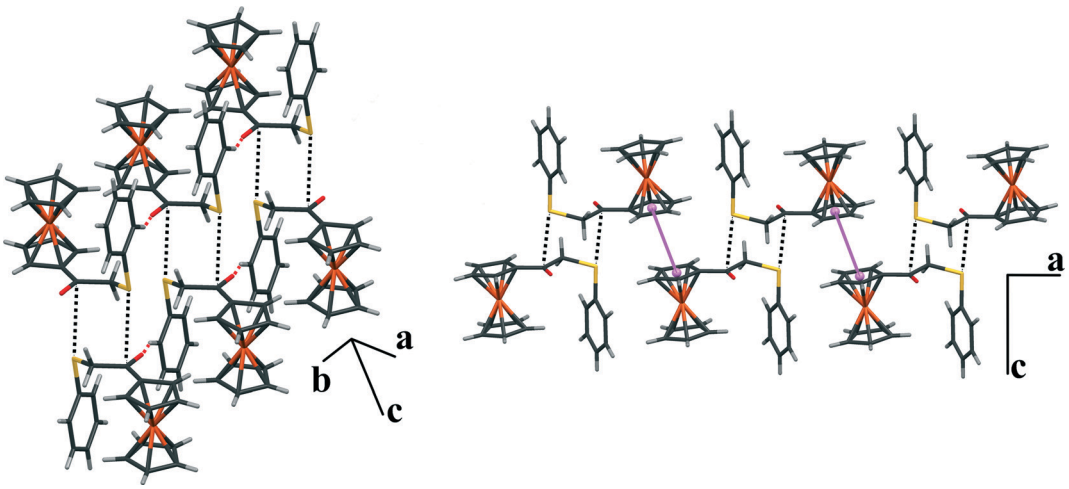

Fig. 6 Double chains of compound **I** molecules along *b*, formed by S–$C_{carbonyl}$ interactions (in black) (left). π–π interactions along *c* are depicted in purple (right).

contacts (Fig. 9). These latter interactions do not result from a large positive point charge in H(19A), but rather from the global positive charge of the methyl group (25 acu%), a situation that can be visualized with the blue area around this group in Fig. 4.

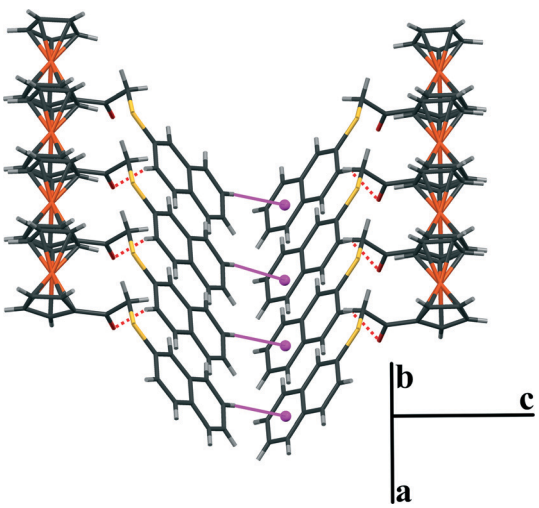

Fig. 7 Chains of compound **II** along *b*, formed *via* C_{aryl}–H···$O_{carbonyl}$ hydrogen bonds (on the left are type I molecules and on the right are type II molecules). C_{aryl}–H···π_{aryl} interchain contacts are represented in purple.

1-Ferrocenyl-2-[3-(methoxyphenyl)thio]ethanone (IV). The main motif in compound **IV** is again C(7) chains along the *b* axis involving C_{Ph}–H···$O_{carbonyl}$ hydrogen bonds (Fig. 10). The choice of H(18) (14 acu%) is not based on electrostatic reasons. H(14) displays a larger point charge value (21 acu%); however, the stereochemical hindrance imposed on the C(14)–H(14) bond by the two *ortho* substituents precludes its participation in the intermolecular contacts.

Due to the relative positioning of the phenyl ring and the methoxy group, the C–H···O chains form a planar network of double chains on plane *ab* with the creation of very stable $R_2^2(8)$ synthons (Fig. 10).

Despite the different secondary motifs, molecules **III** and **IV** display similar packing indexes (71.1 and 70.7%, respectively).

1-Ferrocenyl-2-[4-(chlorophenyl)thio]ethanone (V). In the *para*-chlorophenyl substituted compound (Z' = 2), the most negative point charge is again located in the carbonyl oxygen (−49 and −50 acu%) and not in the chlorine (−15 and −14 acu%), suggesting that the molecules should organize again in linear chains formed by the C_{Cp}–H···$O_{carbonyl}$ interactions both in type 1 and in type 2 molecules. The Cp hydrogen atoms involved (C(10) and C(10A)) are the ones displaying the larger point charges (18 and 17 acu%) in each type of molecule.

These chains grow in opposite directions along *b* and they interact with each other, forming a double chain (Fig. 11).

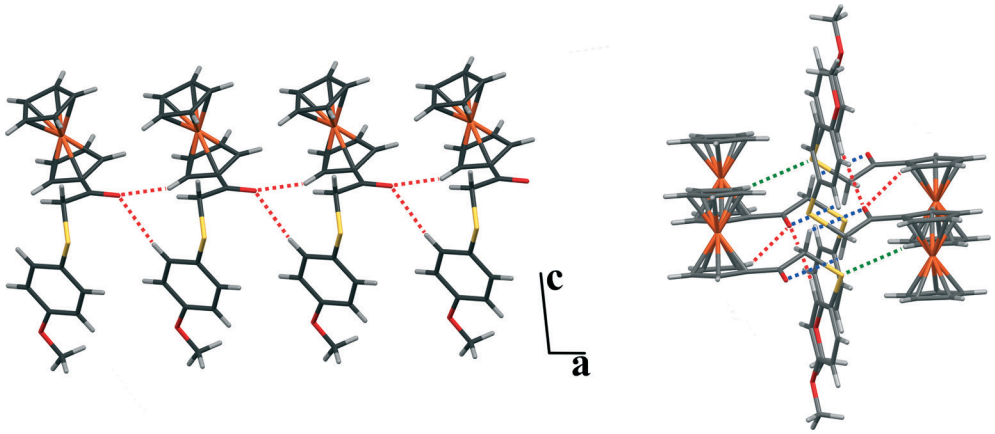

Fig. 8 Chains of molecule **III** along *a* (left), with the C_{Ph}–H···$O_{carbonyl}$ and C_{Cp}–H···$O_{carbonyl}$ hydrogen bonds represented in red; details of the double chains formed through $C_{methylene}$–H···$O_{carbonyl}$ hydrogen bonds (blue) and C_{Cp}–H···S contacts (green) (right).

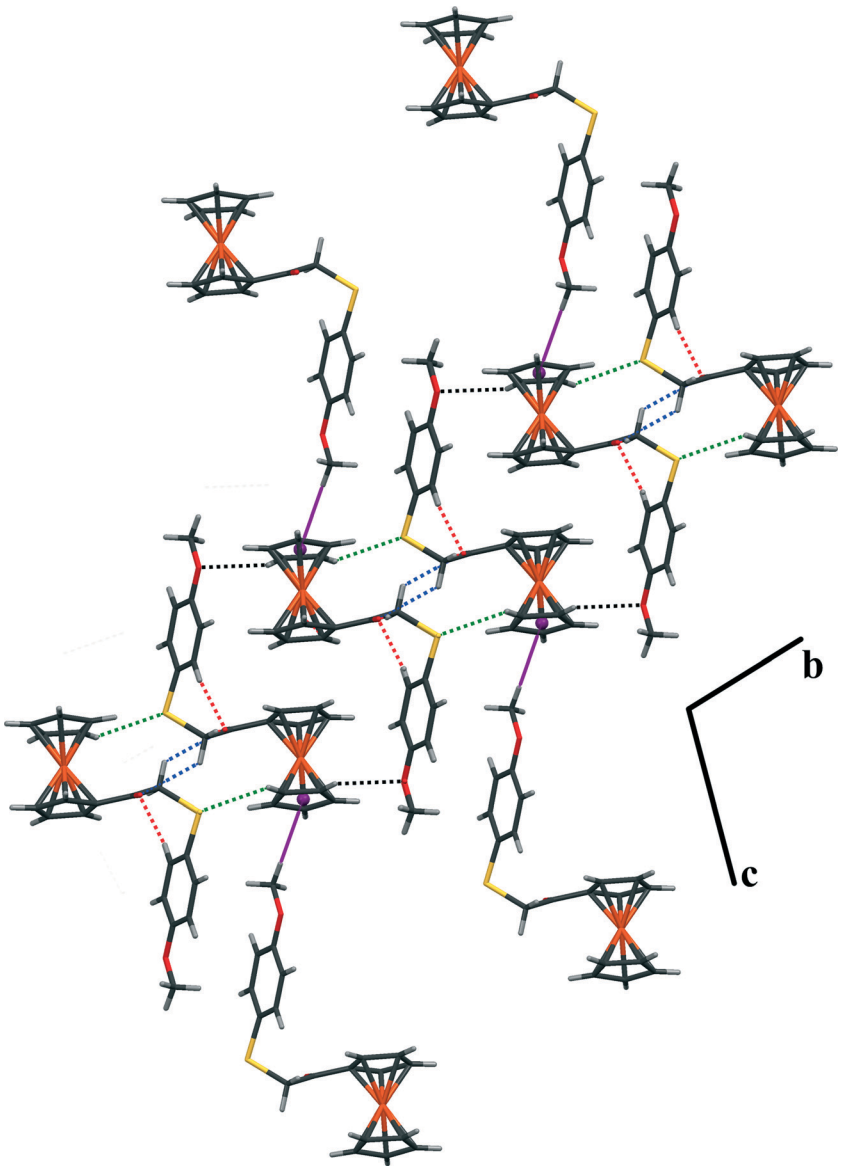

Fig. 9 Supramolecular arrangement of compound **III** on plane *bc*, based on methoxy group interactions: C_{Cp}–H···$O_{methoxy}$ hydrogen bonds (black) and $C_{methoxy}$–H···π_{Cp} contacts (purple).

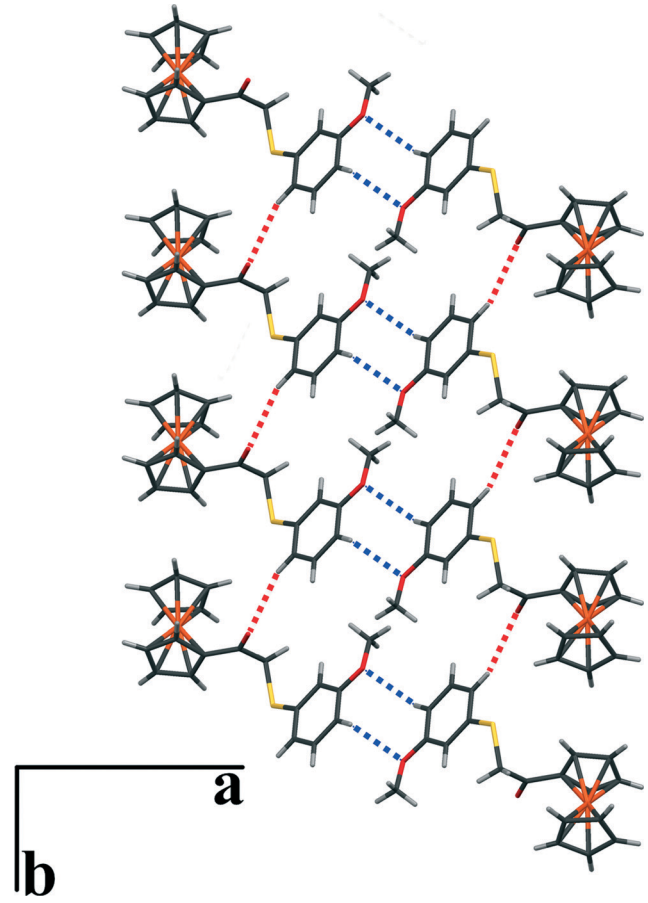

Fig. 10 Supramolecular arrangement of compound **IV** on plane *ab*, formed by C_{Ph}–H···$O_{carbonyl}$ (red) and C_{Ph}–H···$O_{methoxy}$ hydrogen bonds (blue).

This arrangement involves C_{Cp}–H···Cl reinforced by $C_{methylene}$–H···π_{Ph} contacts. The $C_{methylene}$–H···π_{Ph} interactions result from the unusually high point charges for the methylene H(12A) (10 acu%) and H(12D) (11 acu%) and from the relative positioning of the phenyl ring and the ferrocene moiety.

It is worth noting that the values of the H···Cl–C angles are close to 100°, which are in good agreement with study by Glaser *et al.* who reported several C(sp_2)–H···Cl–C(sp_2) interactions with H···Cl distances in the range 3.00–3.41 Å and H···Cl–C angles in the range 79.7–143°.[10]

It is well known that halogen intermolecular contacts heavily depend on the charge density anisotropy around the halogen nuclei.[11,12,17,18] This charge distribution allows the atom to act both as a donor and as an acceptor of electron density. As a donor, it can intervene in C–H···X hydrogen bonds.[18–20] The small angles obtained are in good agreement with a donor–acceptor interaction between the electronegative ring of the halogen and an electronic deficient atom like hydrogen.

The compact arrangement (PI = 70.7%) in **V** is due to both Cl···Cl interactions between molecules in different double chains and the C_{Cp}–H···Cl contacts mentioned above, forming bifurcated bonds involving each chlorine atom. These Cl···Cl contacts display C–X···X angles that fall into Desiraju's definition of type I halogen bonds,[11] with van der Waals interactions between the negative belts of two halogens (see Fig. 12).

1-Ferrocenyl-2-[3-(chlorophenyl)thio]ethanone (VI). The packing of **VI** shows, as a primary motif, a zigzag chain, along *c*, formed by C_{Cp}–H···$O_{carbonyl}$ involving a hydrogen atom from the unsubstituted Cp ring. This chain is shaped not only by these hydrogen bonds but also by bifurcated C–H···π_{Cp} interactions (see Table S3†). The supramolecular motif grows along *b* through bifurcated C–H···Cl between two chains in reversed orientation (Fig. 13).

The role of halogen atoms in directing molecular self-assembly phenomena has been discussed since 1970 (ref. 21) and reported in the literature for various types of halogen (particularly chlorine) contacts.[22] The supramolecular arrangement of **VI** is determined by competition between C–H···O and C–H···Cl hydrogen bonds, and instead of a C–H···O linear chain, a zigzag chain supported by a C–H···Cl network is obtained. This C–H···O zigzag chain no longer involves the hydrogen with the larger electronic point charge

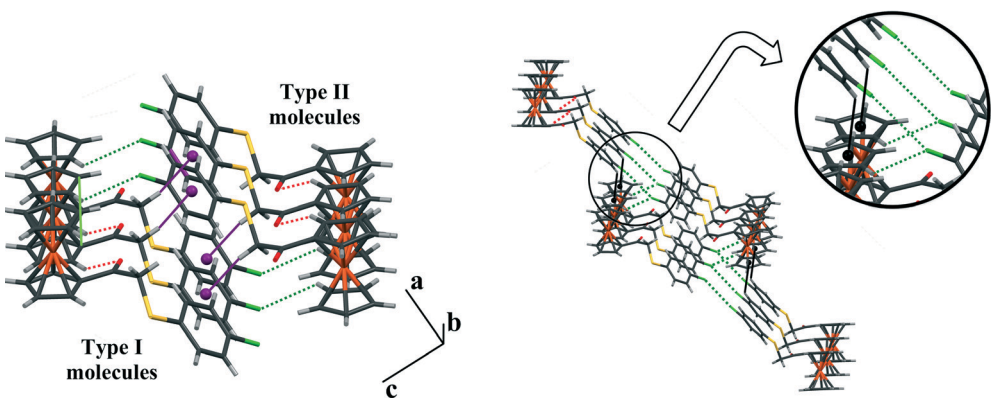

Fig. 11 Double chains of compound **V**: C_{Cp}–H···$O_{carbonyl}$ hydrogen bonds (red), C_{Cp}–H···Cl contacts (green) and $C_{methylene}$–H···π_{Ph} contacts (purple) (left); interaction between two double chains involving bifurcated halogen bonds (interchain Cl···Cl and intrachain C_{Cp}–H···Cl bonds) (right).

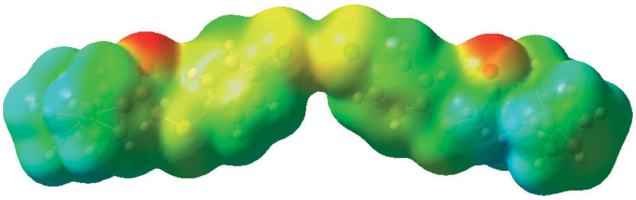

Fig. 12 Electrostatic potential mapped onto an electron density isosurface for the Cl···Cl interaction between two molecules of **V**.

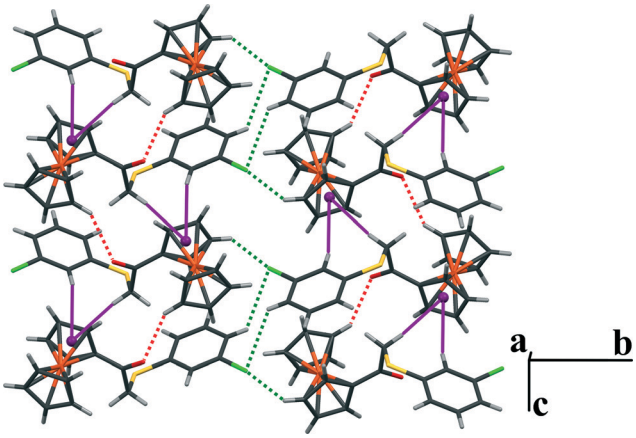

Fig. 13 Supramolecular arrangement of **VI**: zigzag chains formed by C_{Cp}–H···$O_{carbonyl}$ hydrogen bonds (red), C–H···π_{Cp} contacts (purple) and interchain C–H···Cl interactions (green).

((H(10) ~18 acu%) or any other hydrogen (like H(18) ~14 acu%) opposite the carbonyl group, but a hydrogen atom with lower electronic density located in the upper Cp ring (H(1) ~9.5 acu%) (Fig. 13).

1-Ferrocenyl-2-[2-(chlorophenyl)thio]ethanone (VII). As in the previous compound, the driving crystal motif is a zigzag chain formed by C–H···$O_{carbonyl}$ hydrogen bonds, but this time (due to the relative orientation of the chlorophenyl ring and the ferrocene moiety) the bifurcated interactions involve again a hydrogen atom of the unsubstituted Cp and a hydrogen atom of a methylenic moiety.

These chains interact with each other along *b* by C_{Cp}–H···Cl interactions forming a planar arrangement (Fig. 14).

Another planar motif is formed by zigzag chains involving C_{Cp}–H···S interactions, reinforced by C_{Cp}–H···π_{Ph} contacts, and C(9)–H(9)···Cl(1) interactions (Fig. 14). The two planar arrangements form an angle of 108.1° and they interact through C(2)–H(2)···S(1) contacts (see Fig. S4†). Despite the different crystalline arrangements, compounds **VI** and **VII** show PI values (71.0 and 71.3%, respectively) identical to those of the compounds discussed above.

1-Ferrocenyl-2-[4-(nitrophenyl)thio]ethanone (VIII). The nitro group is a good hydrogen acceptor, but the carbonyl oxygen is again the atom with the most negative point charge (−45 and −47 acu% for molecules 1 and 2, respectively, with values of −39 to −40 acu% for the nitro oxygens). Thus, the supramolecular arrangement of compound **VIII** shows, as a primary motif, C_{Cp}–H···$O_{carbonyl}$ C(5) chains, formed separately by type 1 and type 2 molecules ($Z' = 2$) (Fig. 15, red interactions).

The carbonyl oxygen in this compound is actually a bifurcated acceptor, contributing to the formation of ladders of type 1 and type 2 molecules (Fig. 15, blue interactions).

The presence of a strong acceptor, like NO_2, as a substituent in the phenyl ring plays a key role in the final crystal and molecular structures of this compound. In order to achieve more compact packing, this group promotes the interaction between type 1 and type 2 molecules, with the formation of two C_{Cp}–H···O_{nitro} hydrogen bonds between one oxygen of the nitro group and a hydrogen of the unsubstituted Cp ring (Fig. 16). To facilitate these interactions, the two molecules assume an orientation in which the phenyl ring, the bridging group and the substituted Cp are nearly coplanar. The electrostatic potential map of this dimer formation can be visualized in Fig. 16, where the partial charge transfer between the nitro and the unsubstituted Cp groups can be clearly seen.

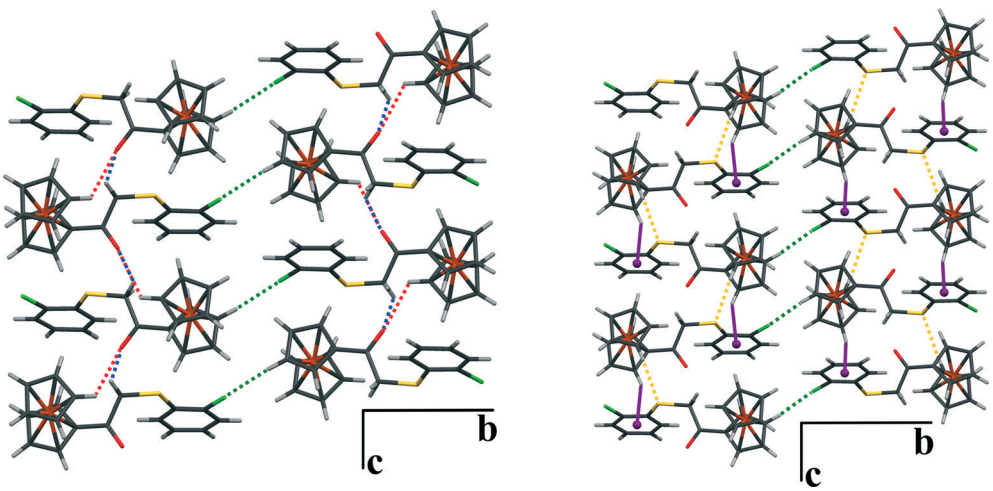

Fig. 14 View along *a* of zigzag chains of compound **VII**: C_{Cp}–H···$O_{carbonyl}$ (red) and $C_{methylene}$–H···$O_{carbonyl}$ (blue) hydrogen bonds (left) and interactions involving C_{Cp}–H···S (yellow) and C_{Cp}–H···π_{Ph} (purple) contacts (right). C_{Cp}–H···Cl interactions are displayed in green.

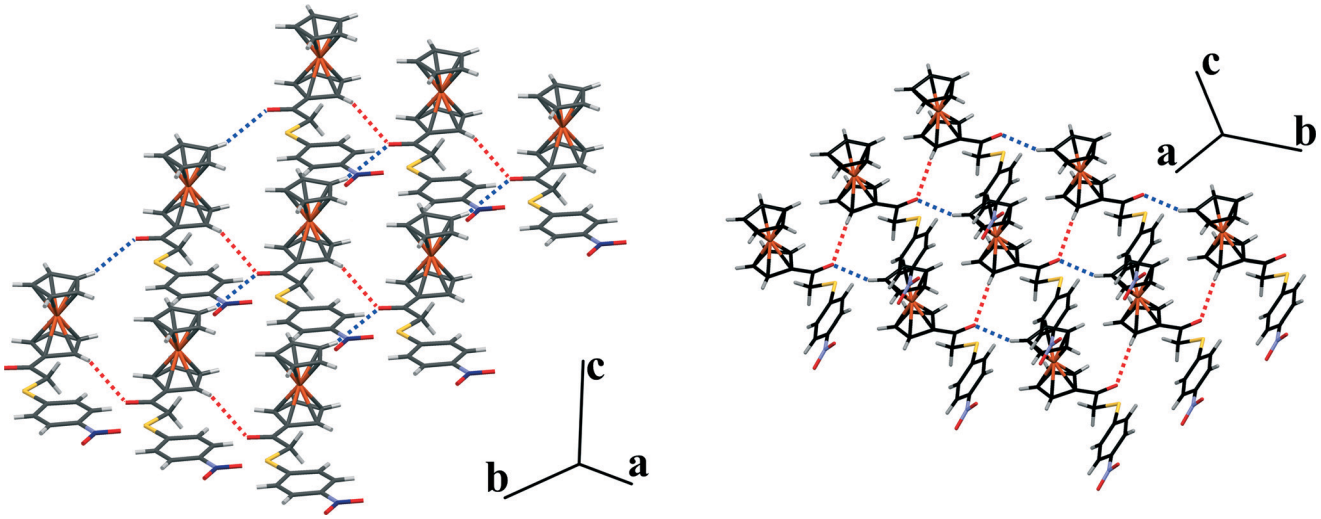

Fig. 15 Ladders of molecules **VIII**-type 1 (left) and **VIII**-type 2 (right), based on C_{Cp}–H···$O_{carbonyl}$ hydrogen bonds.

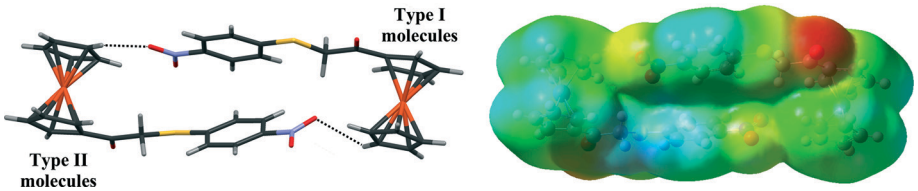

Fig. 16 Interactions between type 1 and type 2 molecules of compound **VIII** (left). Electrostatic potential mapped onto an electron density isosurface for these interactions (right).

Conclusions

The eight compounds studied in the current manuscript display identical functionalities: the ferrocenyl moiety, the oxoethylthio bridge and an aromatic system. The main distinction between them resides in the presence (or the absence) of different substituents in various positions of the aromatic system. It is possible to identify in these molecules five groups that can interact by donor–acceptor recognition processes: the carbonyl group, the sulphur atom, the π-ring systems, the substituent groups and the aromatic C–H bonds. The strongest acceptor present is, undoubtedly, the carbonyl oxygen atom, as confirmed by DFT calculations. Therefore, as the carbon atoms are the only possible hydrogen donors, the primary motifs expected in all supramolecular arrangements are C–H···$O_{carbonyl}$ hydrogen bonds. Based on an electrostatic approach, it is extremely difficult to predict where these bonds should take place, in view of the very similar values of the point charges in the various hydrogen atoms (see Table S2†).

Compounds **I** and **II**, where aryl substituents are absent, display C(7) chains involving C(18)–H(18)···$O_{carbonyl}$ as the primary motif. H(18) does not show the highest point charge among the hydrogen atoms but it is correctly positioned in the molecule inducing the formation of this stable supramolecular arrangement, and allowing complementary intermolecular contacts that stabilize the energetics and reinforce the compactness of the crystal. These C(7) chains are grouped in double chains; in these compounds, further assemblage is promoted by S–C(π)═O and C–H···π contacts.

Compounds **III** and **IV** have a methoxy group in the phenyl ring in *para* and *meta* positions, respectively. From DFT calculations, it could be inferred that the oxygen in this group displays smaller values of negative point charge than that in the carbonyl moiety. So the primary motif will be again C(7) chains, using C(18)–H(18)···$O_{carbonyl}$ hydrogen bonds, in both compounds. The different positioning of the methoxy group dictates different crystal packing arrangements. In **III**, due to its terminal *para* position, the formation of double chains is allowed through C–H···S hydrogen bonds, completing the final 3D structure by means of C_{Cp}–H···$O_{methoxy}$ and $C_{methoxy}$–H···π_{Cp} short contacts. In **IV**, however, the *meta* position of the methoxy group induces the formation of planar double chains, based on $R_2^2(8)$ homosynthons defined by C···H_{phenyl}···$O_{methoxy}$ contacts.

Compounds **V**, **VI** and **VII** present chlorine atoms as phenyl substituents in *para*, *meta*, and *ortho* positions, respectively. The competition between C–H···O and C–H···X hydrogen bonds in directing molecular self-assembly phenomena is well known (particularly for chlorine); to achieve this control over crystallization patterns halogen atoms make use of the high directionality of their interactions. This suggests that competition between C–H···O and C–H···Cl hydrogen bonds will determine the supramolecular arrangement in these compounds.

In compound **V**, chlorine has a lower negative point charge when compared to the carbonyl oxygen, but due to their relative distance, the latter still dictates the primary motif, that is again C–H···O chains. However, the chlorine atoms not only promote the interactions involved in the secondary motifs (C_{Cp}–H···Cl and type I Cl···Cl contacts, forming a double chain) but also cause the involvement of C(10) instead of C(18) in the C–H···O chains in order to facilitate the halogen interactions, achieving an arrangement that is favourable not only in terms of compactness but also energetically due to the larger number of interactions formed.

In compounds **VI** and **VII** this C–H···O and C–H···Cl competition, controlled by the positioning of the chlorine atom together with its greater proximity to the carbonyl group, creates an intercrossing of C–H···O zigzag chains and C–H···Cl chains. However, in these compounds, the hydrogen atom involved in the C–H···O hydrogen bonds is located in the unsubstituted Cp ring and, despite showing low electronic density values, plays a central role in achieving a more compact array.

The absence of Cl–Cl bonds both in **VI** and **VII** may be explained by the large volume and polarizability of the halogen atom when compared to hydrogen. Thus, due to the *meta* and *ortho* positions of the chlorine atom in relation to the thioether substituent, C–H···X hydrogen bonds are favoured over Cl···Cl interactions for steric reasons. This situation does not exist in **V**, in which the greater exposure of the *para*-chlorine atom favors the establishment of type I halogen bonds.

In compound **VIII**, the *para*-nitrophenyl substituted molecule, the effect of the resonance characteristics of the nitro group is immediately shown in the molecular structure of the compound, causing the planarity of the bridge-phenyl-nitro system. DFT calculations also proved that the oxygen atoms in this group as acceptors are not as good as the carbonyl oxygen. This fact creates the conditions for the supramolecular primary motif in **VIII** to be similar to those of compounds **I–IV**. However, instead of C(7) chains containing C(18), the arrangement is built upon C(5) chains involving C(10), which is better placed for this purpose than the C(18) due to the planarity of the aryl moiety. The nitro group acceptor capacity also contributes to the final compact dimers formed by secondary hydrogen bonds with an H from the unsubstituted Cp ring.

In conclusion, the overall crystalline structures of this series of compounds are determined not only by weak C–H···O hydrogen bonds but also by the presence of substituents. These functional groups play an important role in directing the buildup of the crystalline framework, because of their intrinsic donor–acceptor properties and their relative positioning. Certain substituents, such as chlorine, also present distinctive types of interactions that affect the molecular self-assembly phenomena.

The main result arising from the study of the supramolecular arrangements and DFT calculations presented here is that, in molecules in which weak hydrogen bonding is the main driving force, the leading factor in the choice of donor atoms involved in the interactions is not their electron charge but their position in the molecule. This results in the optimization of the crystal packing compacity.

Experimental section

Syntheses

Potassium *t*-butoxide (1.5 equiv.) was added to a solution of benzenethiol (14 mmol) in 30 mL of anhydrous diethyl ether, and the suspension was stirred at room temperature for *ca.* 1 h. 2-Chloro-1-ferrocenylethanone [5.6 g, 1.5 equiv.] was added and the mixture was stirred overnight. The solid materials were then removed by filtration over Celite. The thioether precipitated upon cooling, and the crystals were collected by filtration and dried under vacuum.

The synthesis and spectral characterization (IR, ^{1}H and ^{13}C NMR, and MS) of 1-ferrocenyl-2-[3-(methoxy)phenylthio]-ethanone (**IV**) was reported in our previous study.[1]

The spectral characterization data for the remaining 1-(ferrocenyl)-2-(aryl)thioethanones discussed in the current paper is presented in detail in the ESI† file.

X-Ray crystallographic analysis

X-ray crystallographic data for compounds **I** to **VIII** were collected from crystals using an area detector diffractometer (Bruker AXS-KAPPA APEX II) equipped with an Oxford Cryosystem open-flow nitrogen cryostat at 150 K and graphite-monochromated Mo Kα (λ = 0.71073 Å) radiation. Cell parameters were retrieved using Bruker SMART software and refined with Bruker SAINT[23] on all observed reflections. Absorption corrections were applied using SADABS.[24] The structures were solved by direct methods using SIR 97 (ref. 25) and refined with full-matrix least-squares refinement against F^2 using SHELXL-97.[26] All the programs are included in the WINGX package (version 1.70.01).[27] All non-hydrogen atoms were refined anisotropically, and the hydrogen atoms were inserted in idealized positions, riding on the parent C atom, except for the methoxy hydrogens, whose orientation was refined from electron density, allowing the refinement of both O–C torsion angles and C–H distances. Drawings were made with ORTEP3 for Windows.[28] Geometrical parameters such as average bond lengths, distances to centroids, angles between planes and intramolecular and intermolecular interactions were calculated using Platon 310310.[29] The same interactions were visualized and analysed using Mercury 1.4.2 (Build 2).[30] Compound **VIII** displayed disorder in the C(1A)–C(5A) Cp ring; modelling this disorder led to site occupancy factors (sof) of 0.67(3) and 0.33(3) and anisotropic refinement of these atoms implied the use of EADP constraints; for reasons of intelligibility, atomic fractions with smaller values of sof were omitted in all the figures and tables presented in this work. The correct configuration of **VIII** was confirmed reaching a Flack parameter of 0.09(4). Relevant details of the X-ray data analysis are displayed in

Table 3 Crystal and structure refinement for compounds I–III and V–VIII

	I	II	III	IV	V	VI	VII
$\rho_{calcd.}$ (g cm^{-3})	1.528	1.454	1.508	1.575	1.580	1.594	1.578
Absor. coef. (mm^{-1})	1.169	0.979	1.071	1.266	1.271	1.282	1.086
F_{000}	1392	1600	380	1520	760	760	784
θ range (°)	2.62/27.93	2.92/25.46	3.00/28.42	1.89/25.37	2.49/25.26	3.13/25.74	2.36/25.33
Data collected (h,k,l)	$-24 \le h \le 24$ $-7 \le k \le 7$ $-35 \le l \le 35$	$-7 \le h \le 12$ $-8 \le k \le 8$ $-54 \le l \le 54$	$-7 \le h \le 7$ $-15 \le k \le 15$ $-18 \le l < = 18$	$-29 \le h \le 29$ $-7 \le k \le 7$ $-26 \le l \le 25$	$-9 \le h \le 9$ $-27 \le k \le 28$ $-10 \le l \le 11$	$-8 \le h \le 8$ $-27 \le k \le 28$ $-11 \le l \le 11$	$-7 \le h \le 7$ $-41 \le k \le 35$ $-9 \le l \le 9$
Reflections collected/unique	25 681/3443	15 329/6248	12 012/4047	20 655/5647	12 798/2769	9158/2914	11 966/5232
$R_{(int)}$	0.0770	0.0860	0.0329	0.1109	0.1162	0.0624	0.0881
Completeness to Θ max (%)	98.2	99.2	99.2	99.6	98.1	98.4	99.3
Max./min. transmission	0.7998/0.5406	0.9807/0.6955	0.6740/0.5659	0.6314/0.4307	0.9750/0.8834	0.9748/0.7836	0.9786/0.8121
Data/restraints/parameters	3443/0/190	6248/1/429	4047/0/220	5647/13/398	2769/0/199	2914/0/199	5232/1/429
Goodness-of-fit on F^2	1.032	0.975	1.029	0.756	0.994	1.047	0.957
Final R indices	R_1 = 0.0337	R_1 = 0.0674	R_1 = 0.0281	R_1 = 0.0443	R_1 = 0.0505	R_1 = 0.0513	R_1 = 0.0513
[$I > 2$sigma(I)]	wR_2 = 0.0718	wR_2 = 0.1260	wR_2 = 0.0679	wR_2 = 0.0561	wR_2 = 0.0984	wR_2 = 0.1090	wR_2 = 0.0760
R indices (all data)	R_1 = 0.0509 wR_2 = 0.0779	R_1 = 0.1350 wR_2 = 0.1538	R_1 = 0.033 wR_2 = 0.0708	R_1 = 0.0891 wR_2 = 0.0637	R_1 = 0.1293 wR_2 = 0.1241	R_1 = 0.0841 wR_2 = 0.1203	R_1 = 0.1061 wR_2 = 0.0901
Absolute structure parameter		0.28(3)		0.52(3)			0.09(3)
Extinction coefficient		0.0044(4)					
Largest diff. peak/hole (e Å^{-3})	0.392/−0.299	0.382/−0.345	0.328/−0.252	0.544/−0.418	0.458/−0.497	0.636/−0.475	0.326/−0.582

Table 3. The crystallographic data for compounds **I–III** and **V–VIII** were deposited with the Cambridge Crystallographic Data Centre (CCDC 1044508, 1044509, 1044510, 1044511, 1044512, 1044513, and 1051170).

Ab initio calculations

Electrostatic charge distributions were calculated using Gaussian 03 (ref. 31) at the B3LYP/6-311G(3df,3pd) level of theory. The point charges placed at the center of the mass of each atom in the molecules were calculated from the electronic density function using an electrostatic surface potential methodology (CHelpG). The conformations of the isolated molecules obtained from the crystallographic data were taken as the reference.

Acknowledgements

We thank Conceição Oliveira for obtaining the HRMS data and Agílio A. H. Pádua for allowing access to computer facilities. Thanks are also due to the Portuguese NMR and MS Networks (IST-UL Center) for providing access to the facilities. This work was supported in part by research grants from Fundação para a Ciência e a Tecnologia (FCT), Portugal [UID/QUI/00100/2013, RECI/QEQ-QIN/0189/2012, RECI/QEQ-MED/0330/2012, and FCT-ANR/CTM-NAN/0135/2012], and by a post-doctoral fellowship from FCT to KS (SFRH/BPD/94291/2013).

Notes and references

1 A. P. Ferreira, J. L. Ferreira da Silva, M. T. Duarte, M. F. Minas da Piedade, M. P. Robalo, S. G. Harjivan, C. Marzano, V. Gandin and M. M. Marques, *Organometallics*, 2009, **28**, 5412–5423.
2 G. R. Desiraju, *Acc. Chem. Res.*, 1996, **29**, 441–449.
3 G. R. Desiraju, *Crystal Engineering. The Design of Organic Solids*, Elsevier, Amsterdam, 1989, pp. 142–164.
4 G. R. Desiraju and T. Steiner, *The Weak Hydrogen Bond in structural chemistry and biology*, ed. IUCR, Oxford University Press, Oxford, 1999, pp. 293–338.
5 See [4], pp. 230–231.
6 J. J. Novoa, M. C. Rovira, C. Rovira, J. Veciana and J. Tarrés, *Adv. Mater.*, 1995, **7**, 233–237.
7 J. Lewinski, W. Bury and W. Justtyniak, *Eur. J. Inorg. Chem.*, 2005, **22**, 4490–4492.
8 M. Nishio, Y. Umezawa, K. Honda, S. Tsuboyama and H. Suezawa, *CrystEngComm*, 2009, **11**, 1757–1788.
9 R. R. Choudhury and R. Chitra, *CrystEngComm*, 2010, **12**, 2113–2121.
10 R. Glaser, R. F. Murphy, Y. Sui, C. L. Barnes and S. H. Kim, *CrystEngComm*, 2006, **8**, 372.
11 T. T. T. Bui, S. Dahaoui, C. Lecomte, G. R. Desiraju and E. Espinosa, *Angew. Chem.*, 2009, **121**, 3896–3899.
12 P. Metrangolo, F. Meyer, T. Pilati, G. Resnati and G. Terraneo, *Angew. Chem., Int. Ed.*, 2008, **47**, 6114–6127.
13 F. H. Allen, O. Kennard, D. G. Watson, L. Brammer, A. G. Orpen and R. Taylor, *J. Chem. Soc., Perkin Trans. 2*, 1987, S1–S19.
14 A. G. Orpen, L. Brammer, F. H. Allen, O. Kennard, D. G. Watson and R. Taylor, *J. Chem. Soc., Dalton Trans.*, 1989, S1–S83.
15 A. I. Kitaigorodskii, *Organic Chemical Crystallography*, Consultants Bureau, New York, 1959.
16 G. A. Jeffrey, *An Introduction to Hydrogen Bonding*, Oxford University Press, New York, Oxford, 1997, pp. 21–26.
17 R. Bertania, P. Sgarbossa, A. Venzo, F. Lelj, M. Amati, G. Resnati, T. Pilati, P. Metrangolo and G. Terraneo, *Coord. Chem. Rev.*, 2010, **254**, 677–695.
18 P. Metrangolo, T. Pilati and G. Resnati, *CrystEngComm*, 2006, **8**, 946–947.

19 (*a*) V. R. Vangala, A. Nangia and V. Lynch, *Chem. Commun.*, 2002, 1304–1305; (*b*) C. Glidewell, J. N. Low, J. M. S. Skakle and J. L. Wardell, *Acta Crystallogr., Sect. C: Cryst. Struct. Commun.*, 2005, **61**, o312; (*c*) L. Brammer, E. A. Bruton and P. Sherwood, *Cryst. Growth Des.*, 2001, **1**, 277; (*d*) A. Dey, R. K. R. Jetti, R. Boese and G. R. Desiraju, *CrystEngComm*, 2003, **5**, 248.

20 G. R. Desiraju and R. Parthasarathy, *J. Am. Chem. Soc.*, 1989, **111**, 8725–8726.

21 O. Hassel, *Science*, 1970, **170**, 497–502.

22 I. Csöregh, T. Brehmer, P. Bombicz and E. Weber, *Cryst. Eng.*, 2001, **4**, 343–357 and references therein.

23 *SMART and SAINT: Area Detector Control and Integration Software*, Bruker AXS, Madison, WI, USA, 2004.

24 SADABS: G. M. Sheldrick, *Program for Empirical Absorption Correction of Area Detectors (Version 2.10)*, University of Göttingen, Germany, 2004.

25 A. Altomare, M. C. Burla, M. Camalli, G. L. Cascarano, C. Giacovazzo, A. Guagliardi, A. G. G. Moliterni, G. Polidori and R. Spagna, *J. Appl. Crystallogr.*, 1999, **32**, 115–119.

26 G. M. Sheldrick, *SHELXL-97, a Computer Program for the Refinement of Crystal Structures*, University of Göttingen, Göttingen, Germany, 1997.

27 L. J. Farrugia, WinGX (v1.70.01), *J. Appl. Crystallogr.*, 1999, **32**, 837–838.

28 L. J. Farrugia, ORTEP-3 for Windows (v1.076), based on ORTEP-III (v1.03) by C. K. Johnson, and M. N. Burnett, *J. Appl. Crystallogr.*, 1997, **30**, 565.

29 (*a*) A. L. Spek, *Acta Crystallogr., Sect. A: Found. Crystallogr.*, 1990, **46**, C34; (*b*) A. L. Spek, *PLATON, A Multipurpose Crystallographic Tool*, Utrecht University, Utrecht, The Netherlands, 1998.

30 I. J. Bruno, J. C. Cole, P. R. Edgington, M. Kessler, C. F. MacRae, P. McCabe, J. Pearson and R. Taylor, *Acta Crystallogr., Sect. B: Struct. Sci.*, 2002, **58**, 389–397.

31 M. J. Frisch, G. W. Trucks, H. B. Schlegel, G. E. Scuseria, M. A. Robb, J. R. Cheeseman, J. A. Montgomery Jr., T. Vreven, K. N. Kudin, J. C. Burant, J. M. Millam, S. S. Iyengar, J. Tomasi, V. Barone, B. Mennucci, M. Cossi, G. Scalmani, N. Rega, G. A. Petersson, H. Nakatsuji, M. Hada, M. Ehara, K. Toyota, R. Fukuda, J. Hasegawa, M. Ishida, T. Nakajima, Y. Honda, O. Kitao, H. Nakai, M. Klene, X. Li, J. E. Knox, H. P. Hratchian, J. B. Cross, V. Bakken, C. Adamo, J. Jaramillo, R. Gomperts, R. E. Stratmann, O. Yazyev, A. J. Austin, R. Cammi, C. Pomelli, J. W. Ochterski, P. Y. Ayala, K. Morokuma, G. A. Voth, P. Salvador, J. J. Dannenberg, V. G. Zakrzewski, S. Dapprich, A. D. Daniels, M. C. Strain, O. Farkas, D. K. Malick, A. D. Rabuck, K. Raghavachari, J. B. Foresman, J. V. Ortiz, Q. Cui, A. G. Baboul, S. Clifford, J. Cioslowski, B. B. Stefanov, G. Liu, A. Liashenko, P. Piskorz, I. Komaromi, R. L. Martin, D. J. Fox, T. Keith, M. A. Al-Laham, C. Y. Peng, A. Nanayakkara, M. Challacombe, P. M. W. Gill, B. Johnson, W. Chen, M. W. Wong, C. Gonzalez and J. A. Pople, *Gaussian 03, revision C.05*; Gaussian, Inc.: Wallingford, CT, 2004.

